Electronic Supplementary Information

Computational Chemistry-Assisted Design of Non-Fullerene Acceptor Enables 17.4% Efficiency in High-Boiling-Point Solvent Processed Binary Organic Solar Cells

Guilong Cai,‡[a] Zeng Chen,‡[b] Tengfei Li,[c] Xinxin Xia,[a] Yuang Fu,[a] Luhang Xu,[a] Weijie Chi*[d], Jianqi Zhang,[e] Haiming Zhu*[b], Xiaowei Zhan,[c] and Xinhui Lu*[a]

[a] Department of Physics, The Chinese University of Hong Kong, New Territories 999077, Hong Kong, China. E-mail: xinhui.lu@cuhk.edu.hk

[b] State Key Laboratory of Modern Optical Instrumentation, Key Laboratory of Excited State Materials of Zhejiang Province, Department of Chemistry, Zhejiang University, Hangzhou 310027, Zhejiang, China. E-mail: hmzhu@zju.edu.cn

[c] School of Materials Science and Engineering, Peking University, Beijing 100871, China.

[d] School of Science, Hainan University, Haikou 570228, China. E-mail: weijie_chi@hainanu.edu.cn

[e] CAS Key Laboratory of Nanosystem and Hierarchical Fabrication, CAS Center for Excellence in Nanoscience, National Center for Nanoscience and Technology, Beijing 100190, China.

Materials

Unless stated otherwise, all the chemical reagents and solvents used were obtained commercially and were used without further purification. Chlorobenzene (99.8%) and 1,8-diiodooctane (DIO) (97.0%) were purchased from Sigma-Aldrich. PM6 (M_n = 20.2 kg mol^{-1}, M_w/M_n = 2.0), 2ClIC and PNDIT-F3N were purchased from OptiFocus Ltd. L8-BO was synthesized according to the reported procedures.[S1]

Synthesis of BOEH-4Cl

BOEH-4Cl. To a three-necked round bottom flask were added BOEH-CHO (106 mg, 0.1 mmol), 2ClIC (92 mg, 0.35 mmol), pyridine (0.15 mL) and chloroform (20 mL). The mixture was deoxygenated with nitrogen for 20 min and then stirred at reflux for 12 h. After cooled to room temperature, the mixture was poured into methanol (200 mL) and filtered. The residue was purified by column chromatography on silica gel using a mixture solvent as eluent (petroleum ether/dichloromethane, v/v = 1/1) to give a blue solid (127 mg, 87%). ^{1}H NMR (400 MHz, CD_3Cl): δ 9.2 (s, 2H), 8.8 (s, 2H), 8.0 (s, 2H), 4.8 (d, J = 7.9 Hz, 4H), 3.2 (d, J = 7.6 Hz, 4H), 2.1 – 2.0 (m, 4H), 1.3 – 1.2 (m, 48H), 0.9 – 0.8 (m, 24H). MS (MALDI-TOF): m/z 1546.2 (M^+).

Characterization

The ^{1}H NMR spectra were measured by Bruker AVANCE 400 MHz spectrometer. Mass spectra were performed by Bruker Daltonics Biflex III MALDI-TOF Analyzer in the MALDI mode. The ultraviolet-visible light (UV-vis) absorption spectra were measured using the JASCO-570 spectrophotometer (JASCO. Inc., Japan) in solution (chlorobenzene) and the thin film (on a quartz substrate). Ultraviolet photoelectron

spectroscopy (UPS) spectra were obtained from AXIS ULTRA DLD (Kratos) with He I (21.22 eV) excitation lines and a sample bias of –9 V under a vacuum of 3.0×10^{-8} Torr. The active layer surface was characterized in ambient conditions via an atomic force microscope (AFM) (Bruker, Dimension Icon) using a platinum–iridium (Pt–Ir) coating tip (Bruker: SCM-PIC-V2; k: 3 N/m; f_0: 75 kHz). The scan area and speed were 2.0 μm × 2.0 μm and 0.6 Hz.

Computational method

DFT calculations were adopted to study the structure and electronic properties of BOEH-4Cl and L8-BO. All geometry optimizations in the ground states were carried out with B3LYP functional in combination with the Def2SVP basis set. Frequency analysis was performed to confirm that we had obtained stable structures on the potential energy surfaces. The SMD solvation model (in chloroform) and the empirical dispersion correction (D3) were considered in all calculations. The excited-state calculations of BOEH-4Cl and L8-BO have been done at the same level. The absorption peaks of Y6 derivatives can be reliably calculated with B3LYP functional, which has been demonstrated (J. Phys. Chem. Lett. 2022, 13, 916−922). For simplicity, a repetitive unit (163 atoms) of the donor polymer was simulated. All calculations were carried out with Gaussian 16 A. The electrostatic potential surface analysis of accepter and donor was carried out with Multifwn_3.7 code and VMD.

Device fabrication

All the devices are based on a conventional sandwich structure, patterned ITO glass/PEDOT:PSS/active layer/ PNDIT-F3N/Ag. The ITO substrates were first

scrubbed by detergent and then sonicated with deionized water, acetone and isopropanol subsequently, and dried in an oven. The glass substrates were treated by UV-ozone for 20 min before use. PEDOT:PSS (Heraeus Clevios P VP AI 4083) was spin-cast onto the ITO substrates at 4000 rpm for 30 s, and then dried at 120 °C for 20 min in air. The donor/acceptor blends (1/1.2 weight ratio, total concentration is 20 mg mL^{-1}) were dissolved in a chlorobenzene and stirred overnight at room temperature in a nitrogen-filled glove box. The blend solution was spin-cast at 2500 rpm for 30 s. Active layers were annealed on a 100 °C hotplate for 10 minutes after being coated. A thin PNDIT-F3N layer (~5 nm) was coated on the active layer, followed by the deposition of Ag electrode (100 nm). The cathode of Ag was deposited by thermal evaporation with a shadow mask under 10^{-4} Pa and the thickness of 100 nm was monitored by a quartz crystal microbalance. The *J-V* curves was measured using a computer-controlled B2912A Precision Source/Measure Unit (Agilent Technologies, United States). An XES-70S1 (SAN-EI Electric Co., Ltd., Japan) solar simulator (AAA grade, 70 mm × 70 mm) coupled with AM 1.5G solar spectrum filters was used as the light source, and the optical power at the sample was 100 mW cm^{-2}. The measured area of the active device was 4 mm^2. A 2 cm × 2 cm monocrystalline silicon reference cell (SRC-1000-TC-QZ) was purchased from VLSI Standards Inc. The external quantum efficiency (EQE) spectra were measured using a Solar Cell Spectral Response Measurement System QE-R3011 (Enlitech Co., Ltd.). The light intensity at each wavelength was calibrated through standard single crystal Si photovoltaic cell.

GIWAXS and GISAXS measurements. GIWAXS and GISAXS measurements were

carried out with a Xeuss 2.0 SAXS/WAXS laboratory beamline using a Cu X-ray source (8.05 keV, 1.54 Å) and a Pilatus3R 300K detector. The incidence angle is 0.15° and 0.2°, respectively. All measurements were conducted under a vacuum environment to reduce air scattering.

Transient Absorption Spectroscopy (TAS) Measurement. For femtosecond transient absorption spectroscopy, the fundamental output from Yb:KGW laser (1030 nm, 220 fs Gaussian fit, 100 kHz, Light Conversion Ltd) was separated to two light beams. One was introduced to NOPA (ORPHEUS-N, Light Conversion Ltd) to produce a certain wavelength for pump beam (here we use 750 nm), the other was focused onto a YAG plate to generate white light continuum as probe beam. The pump and probe overlapped on the sample at a small angle less than 10°. The transmitted probe light from sample was collected by a linear CCD array. Then we obtained transient differential transmission signals by equation shown below:

$$\frac{\Delta T}{T} = \frac{T_{pump\text{ - }on} - T_{pump\text{ - }off}}{T_{pump\text{ - }off}}$$

All the samples were measured in vacuum environments.

Photoluminescence Spectra (PL). Steady-state PL were detected using a home-setup microfluorescence system. The excitation light was 532nm and the PL spectra were measured using a spectrograph (Princeton Instruments) with an EMCCD. All the samples were measured in vacuum environments.

Dielectric constant and Urbach energy measurements. For dielectric constant measurements, a –2 V DC bias was applied to the device under dark to ensure the

complete depletion of free charge carriers. On top of that, a 10 mV AC bias was applied to the device with frequencies ranging between 1 kHz and 1 MHz to obtain the geometric capacitance of neat acceptor films and their blend films with PM6 via the following equation:

$$C_{\mathrm{g}} = -\frac{1}{\omega}\left[\frac{Z'' - \omega L}{\left(Z' - R_S\right)^2 + \left(Z'' - \omega L\right)^2}\right]$$

where Z' and Z'' are the real and imaginary parts of the complex impedance, respectively. ω is the angular frequency of the AC bias applied. R_s is the series resistance of the device obtained from saturation of Z' at high frequency and L is the parasitic inductance. The dielectric constants of neat and blend materials are derived from their respective geometric capacitances via:

$$\varepsilon = \frac{C_g d}{\varepsilon_0 A}$$

where d is the active layer thickness (50 nm for neat films and 100 nm for blend films) and A is the active layer area (4 mm^2).

For Urbach energy measurements, the device is illuminated under background light with various intensities and a DC bias is applied to ensure the device is always under open-circuit conditions. Capacitance measurements were performed under different light intensities and thus different V_{OC}. Subtracting the saturated capacitance at low frequency with the geometric capacitance gives the chemical capacitance associated with charge carriers stored in the active layer. The Urbach energy of the active layer can be obtained via the following equation**:**

$$C\mu \propto exp\left((qV_{oc})/2E_{ch}\right)$$

Supporting Figures

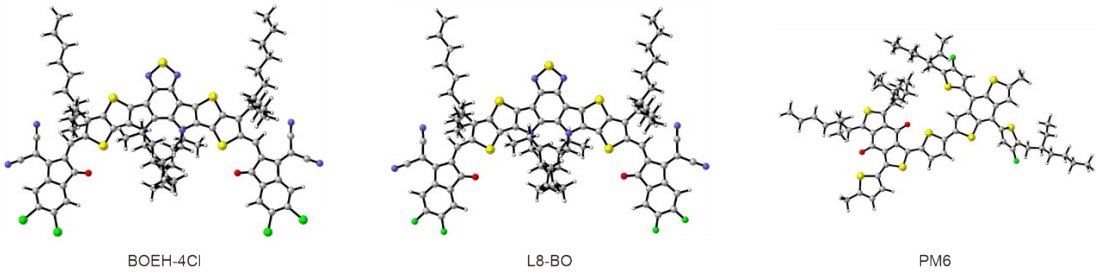

Fig. S1 Optimized molecular structures of BOEH-4Cl, L8-BO, and PM6 at B3LYP/Def2SVP level.

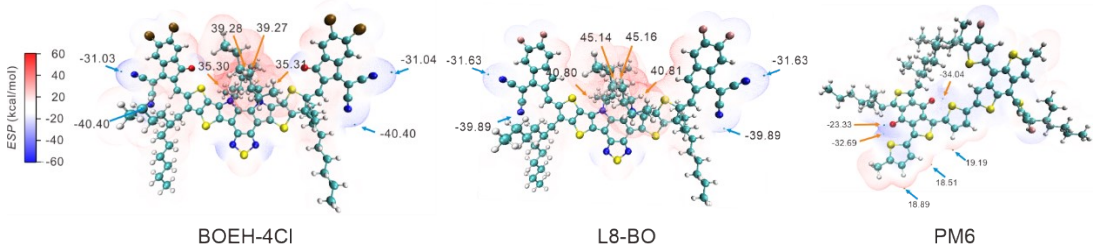

Fig. S2 Calculated the distribution of electrostatic potential surface in BOEH-4Cl, L8-BO, and PM6 at B3LYP/Def2SVP level.

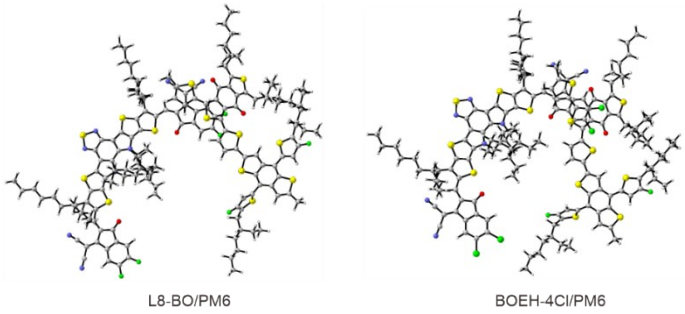

Fig. S3 Optimized molecular structures of BOEH-4Cl/PM6 and L8-BO/PM6 at B3LYP/Def2SVP level.

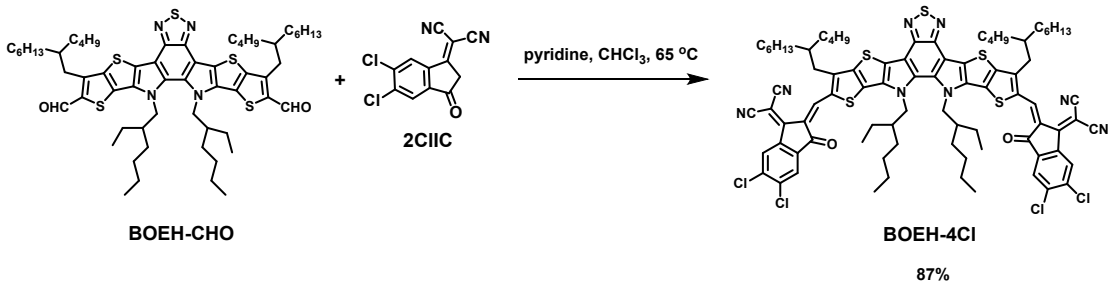

Scheme S1 Synthetic routes to BOEH-4Cl.

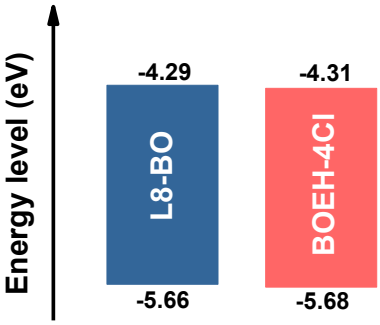

Fig. S4 Energy level diagram.

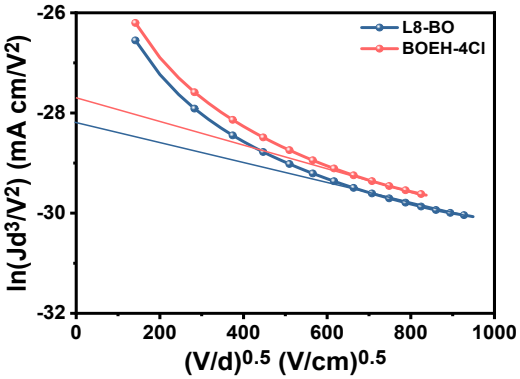

Fig. S5 *J-V* characteristics in the dark for electron-only devices based on pure films.

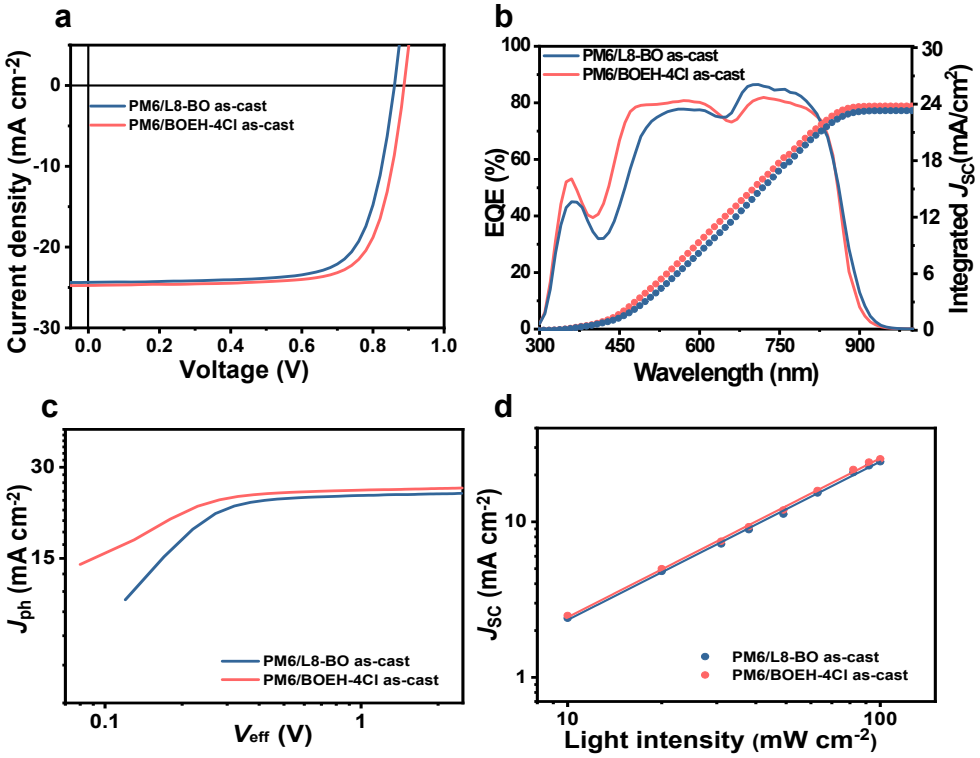

Fig. S6 (a) *J*–*V* curves. (b) EQE response and integrated J_{SC} of best-performing devices. (c) J_{ph} versus V_{eff} characteristics and (d) J_{SC} versus light intensity of the devices.

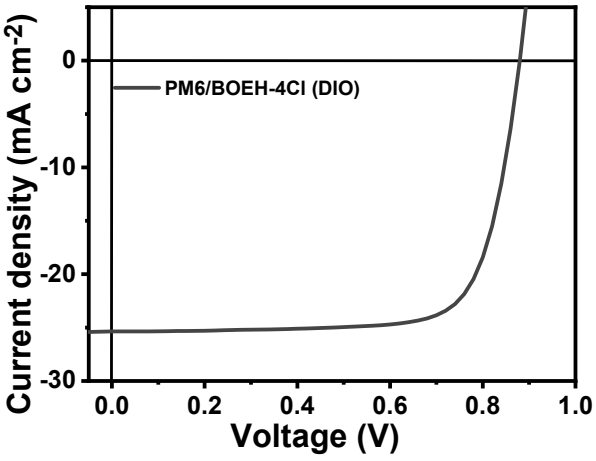

Fig. S7 *J*–*V* curve of PM/BOEH-4Cl (DIO).

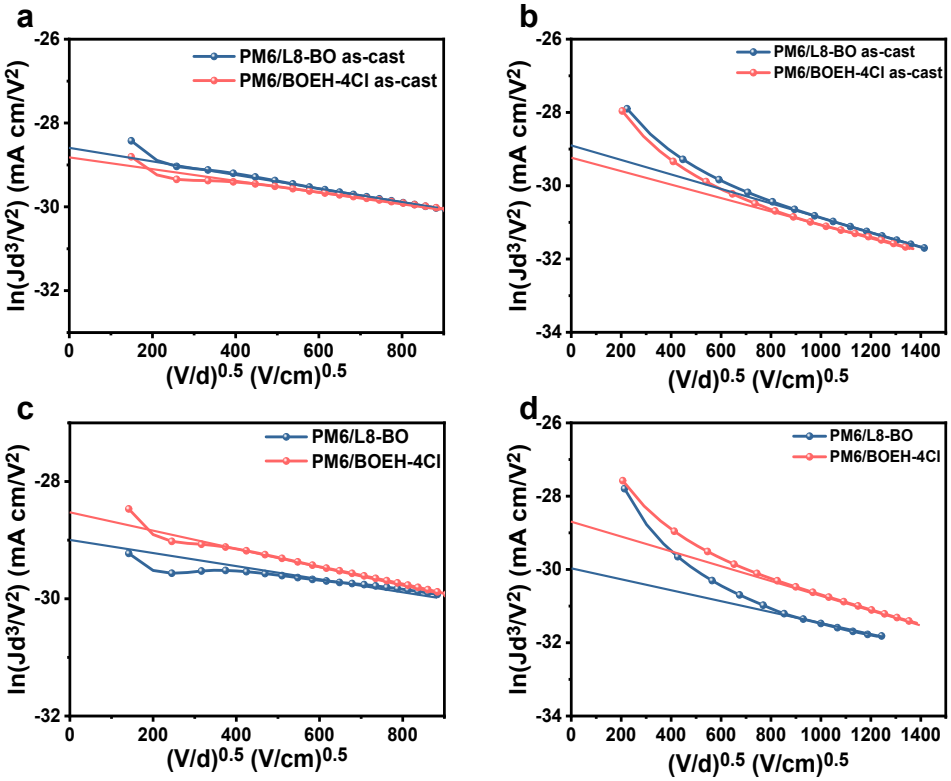

Fig. S8 *J-V* characteristics in the dark for (a,c) hole-only and (b,d) electron-only devices based on optimal binary blends.

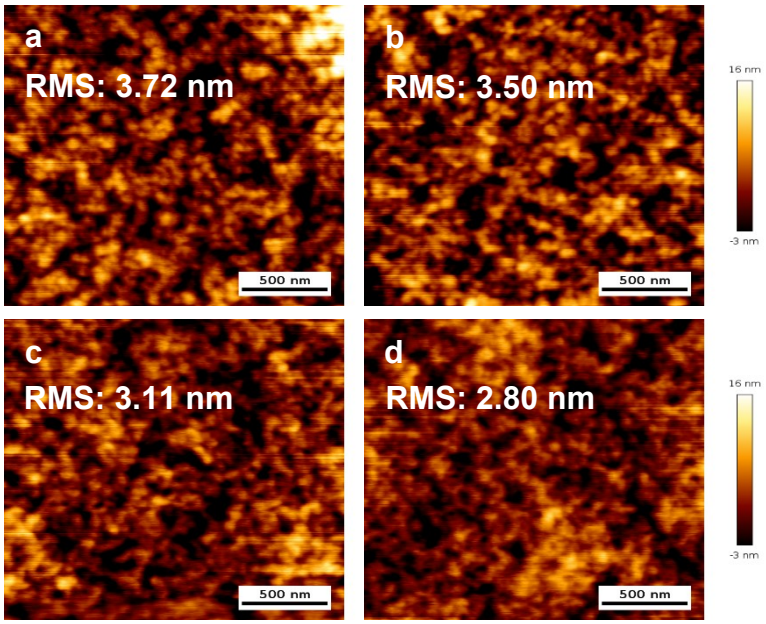

Fig. S9 AFM height images of (a,c) PM6/L8-BO and (b,d) PM6/BOEH-4Cl blend films under as-cast and optimal device conditions, respectively.

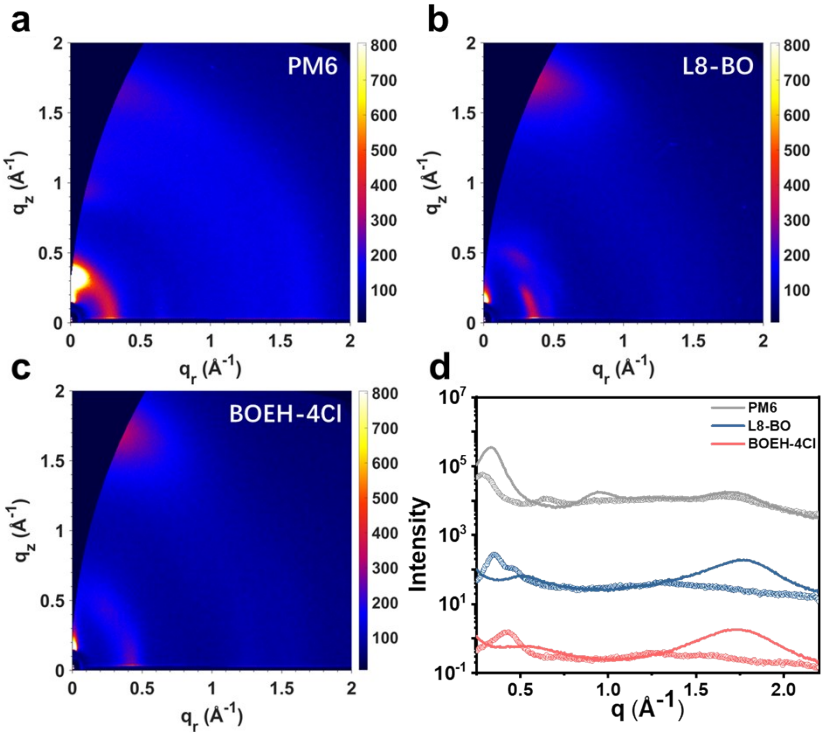

Fig. S10 2D GIWAXS patterns of (a) PM6, (b) L8-BO, (c) BOEH-4Cl and (d) intensity profiles along the IP (dashed line) and OOP (solid line) directions of pure films.

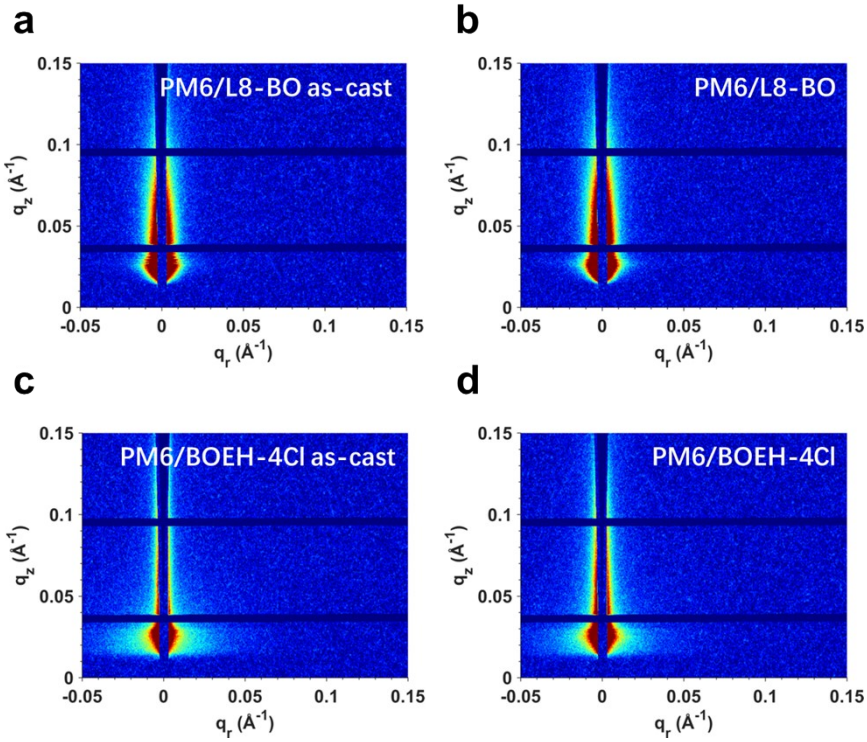

Fig. S11 2D GISAXS patterns of the blends.

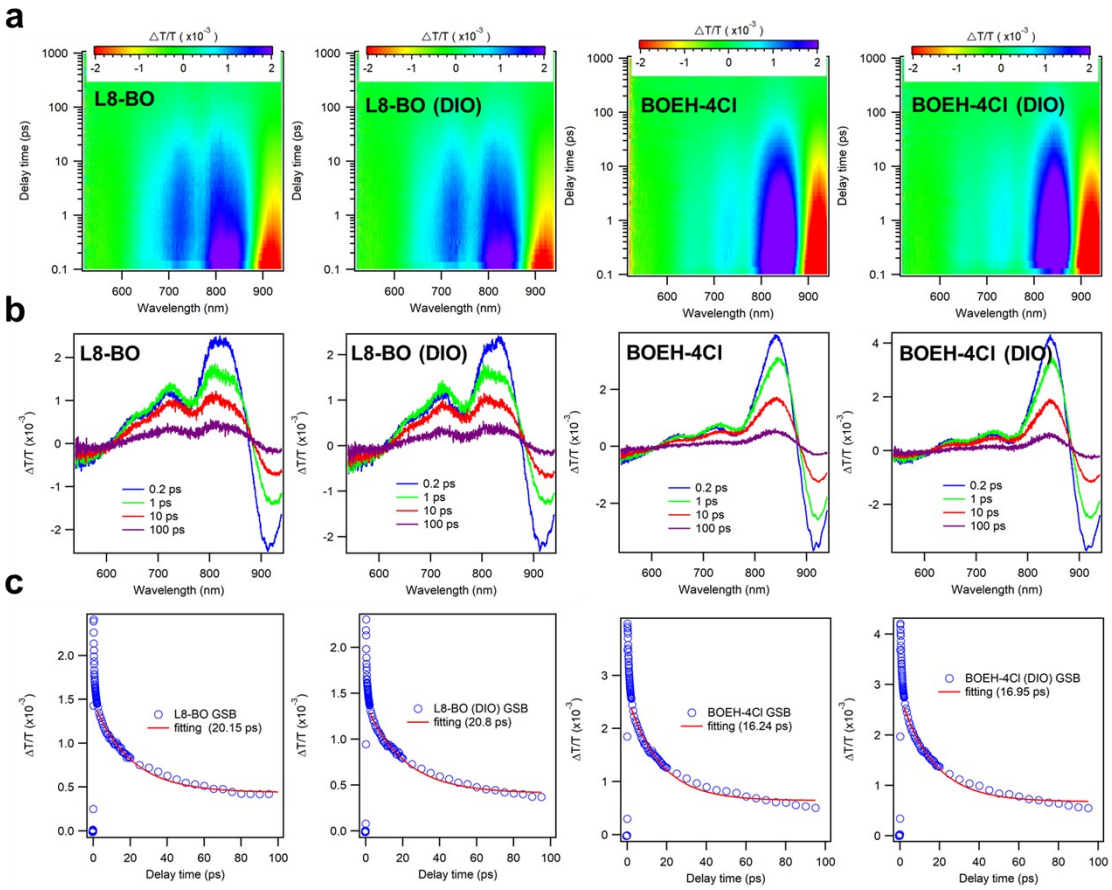

Fig. S12 (a) 2D color plot of fs TA spectra of neat films under 750 nm excitation with a fluence below 5 μJ cm^{-2}. (b) Representative fs TA spectra at indicated delay times. (c) GSB decay kinetics.

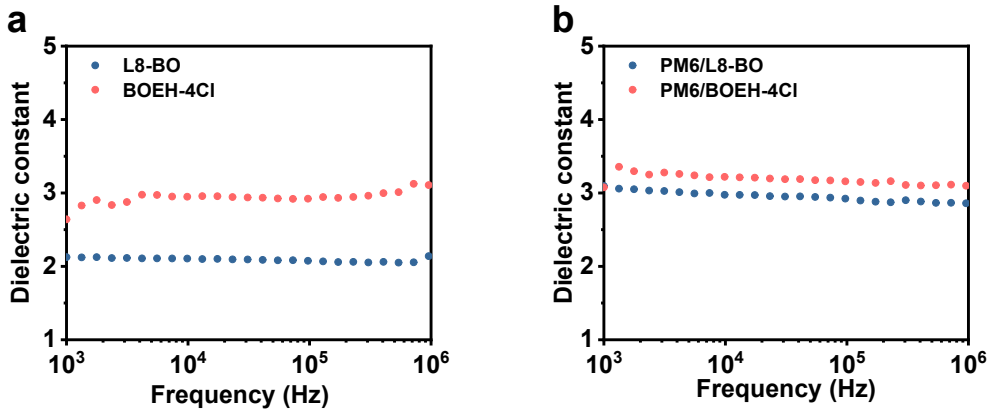

Fig. S13 Dielectric constants of (a) L8-BO and BOEH-4Cl neat films and (b) their respective blend films with PM6 measured by capacitance spectroscopy under dark and reverse bias (–2 V).

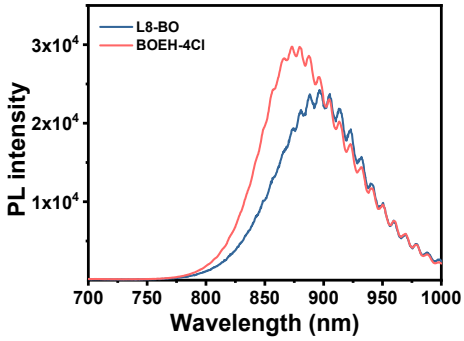

Fig. S14 PL results of L8-BO and BOEH-4Cl neat films under 532 nm excitation.

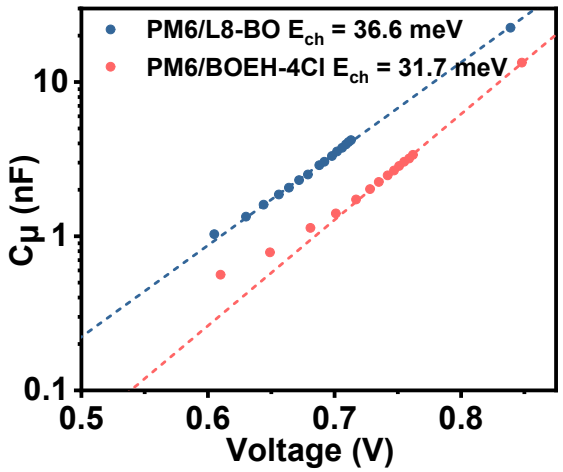

Fig. S15 The change in chemical capacitance (C_μ) with different V_{OC} measured under different background light intensities.

Supporting Tables

Table S1 The parameters of exciton dissociation efficiency and charge collection efficiency

Sample	J_{sat} (mA cm^{-2})	$J_{ph}{}^{a}$ (mA cm^{-2})	$J_{ph}{}^{b}$ (mA cm^{-2})	η_{diss} (%)	η_{coll} (%)
PM6/L8-BO as-cast	24.7	24.4	22.1	98.8	89.5
PM6/BOEH-4Cl as-cast	25.7	24.8	22.3	96.5	86.8
PM6/L8-BO	24.5	23.9	21.4	97.6	87.4
PM6/BOEH-4Cl	26.9	25.6	23.5	95.2	87.4

[a] Under short circuit condition; [b] Under the maximal power output condition.

Table S2 Charge mobilities of pure and blend films measured by SCLC Method

Active layer	μ_h ($\times 10^{-3}$ cm^2 V^{-1} s^{-1})	μ_e ($\times 10^{-3}$ cm^2 V^{-1} s^{-1})	μ_h/μ_e
L8-BO	-	3.3	-
BOEH-4Cl	-	5.5	-
PM6/L8-BO as-cast	2.24	1.66	1.4
PM6/BOEH-4Cl as-cast	1.84	1.23	1.5
PM6/L8-BO	1.50	0.61	2.5
PM6/BOEH-4Cl	2.48	2.03	1.2

Table S3 Calculated GIWAXS characteristics in the OOP direction

Sample	q (Å^{-1})	*d*-spacing (Å)	FWHM (Å^{-1})	CCL (Å)
PM6/L8-BO as-cast	1.72	3.65	0.374	15.1
PM6/L8-BO	1.74	3.61	0.345	16.4
PM6/BOEH-4Cl as-cast	1.71	3.67	0.403	14.0
PM6/BOEH-4Cl	1.72	3.65	0.384	14.7

Table S4 Morphology parameters fitted by GISAXS profiles (ξ is the intermixing domain size; $2R_{g\text{-}fractal}$ is the acceptor domain size)

Sample	ξ (nm)	$2R_g$ (nm)
PM6/L8-BO as-cast	29.3	14.6
PM6/L8-BO	31.9	10.8
PM6/BOEH-4Cl as-cast	29.7	7.2
PM6/BOEH-4Cl	27.5	6.4

Table S5 Hole transfer fitting results ($I = A_1 \exp(-t/\tau_1) + A_2 \exp(-t/\tau_2)$)

Sample	A_1	τ_1 (ps)	A_2	τ_2 (ps)
PM6/L8-BO as-cast	0.585	0.163±0.008	0.415	11.087±0.554
PM6/L8-BO	0.585	0.158±0.008	0.415	11.632±0.582
PM6/BOEH-4Cl as-cast	0.558	0.159±0.008	0.442	5.697±0.285
PM6/BOEH-4Cl	0.530	0.148±0.007	0.470	5.942±0.297

Supporting References

S1 C. Li, J. D. Zhou, J. L. Song, J. Q. Xu, H. T. Zhang, X. N. Zhang, J. Guo, L. Zhu, D. H. Wei, G. C. Han, J. Min, Y. Zhang, Z. Q. Xie, Y. P. Yi, H. Yan, F. Gao, F. Liu, Y. M. Sun, *Nat. Energy* 2021, **6**, 605.